Scripta Materialia 155 (2018) 94–98

Contents lists available at ScienceDirect

Scripta Materialia

journal homepage: www.elsevier.com/locate/scriptamat

Regular article

Ultra-high strength and ductility from rolling and annealing of a Ni-Cr-Co superalloy

C.E. Slone, J. Miao, M.J. Mills *

[a] Center for Electron Microscopy and Analysis, The Ohio State University, Columbus, OH 43212, USA
[b] Department of Materials Science and Engineering, The Ohio State University, Columbus, OH 43210, USA

ARTICLE INFO

Article history:
Received 16 May 2018
Received in revised form 8 June 2018
Accepted 12 June 2018
Available online xxxx

Keywords:
Superalloy
Precipitation
Deformation structure
Work hardening
Recrystallized microstructure

ABSTRACT

A new processing route is demonstrated for producing a nickel-based alloy with 1099 MPa tensile yield strength and 30% elongation. A chromium- and cobalt-rich commercial alloy was solution-annealed, cold-rolled, and aged at different temperatures and times to develop partially-recrystallized microstructures with ordered $Ni_3(Al,Ti)$ γ′ precipitates. These were tested in uniaxial tension and compared to alloys given the same heat treatment without rolling to assess the contributions of different strengthening mechanisms. Orientation mapping showed the development of a modest ⟨111⟩ and ⟨100⟩ double-fiber texture. Scanning transmission electron microscopy also revealed the development of exceptionally large dislocation densities including wall structures.

The last two decades have produced substantial progress in developing materials with outstanding combinations of high strength and ductility, largely through research involving twinning-induced plasticity (TWIP) and transformation-induced plasticity (TRIP) steels [1–3] and more recently "high-entropy" multi-principal element (MPE) alloys [4–6]. It is now common for these alloys to attain ultimate true tensile strengths exceeding 1200 MPa while retaining >30% elongation to fracture. Recent attention has therefore been extended to increasing the yield strengths of these alloys, which often remain in the more modest range of 400–600 MPa [7–10].

Most efforts to enhance room-temperature yield strength have focused on changes in processing and chemistry that exploit mechanisms like deformation twinning. In TWIP steels, one successful avenue involves cold-rolling the material to produce a microstructure with a high density of deformation nanotwins and subsequently annealing at a moderate temperature. The recovery during the annealing step is thought to reduce the dislocation density (thereby restoring some ductility) while the deformation twins, which are stable up to ~625 °C, remain unaffected [11]. The twinning substructure then substantially enhances the yield strength of the alloy on further testing. Using this method, TWIP and TWIP-TRIP steels have exhibited outstanding combinations of yield strength and elongation of, for example, 798 MPa/41% [12] and 1140 MPa/7% [13].

In contrast, yield strength enhancement in MPE alloys has primarily focused on changes in composition. The early emphasis in MPE alloys was on compositions that avoided precipitation of deleterious, embrittling phases and derived their strength from solid solution hardening. This produced alloys like single-phase equimolar FeNiCoCrMn [14] and CrCoNi [15], which have high work-hardening rates and excellent ductility like the baseline TWIP alloys. However, very recent work has shown that conventional precipitation hardening in MPE alloys using the B2 [16] or γ′ phases [17, 18] can significantly enhance the yield strength with only marginal compromises in ductility. The composition chosen by Zhao et al. in [18] is particularly interesting as a derivative of equimolar CrCoNi, which exhibits exceptionally high hardening rates due to formation of nanoscale HCP regions along deformation twins and stacking faults [19, 20].

In this work, we combine processing lessons from TWIP-TRIP alloys with the compositional benefits conferred by the CrCoNi + (Al,Ti) composition space. The alloy chosen for study was commercially available Inconel 740H, which has the nominal composition (in wt%) Ni – 25Cr – 20Co – 1.35Al – 1.35Ti – 1.5Nb – 0.1Mo. This corresponds to an atomic composition of approximately $Ni_{48.5}Cr_{27.0}Co_{19.0}Nb_{0.9}Ti_{1.6}Al_{2.8}Mo_{0.1}$. This composition has several advantages: 1) large Cr and Co contents reduce the stacking fault energy of the alloy and produce a composition similar to thoroughly-studied equimolar CrCoNi; 2) additions of Al and Ti enable precipitation of the well-known γ′ phase that has been thoroughly studied in Ni-based superalloys; and 3) the (Al + Ti) content is low so precipitation can be avoided with a fast quench from the solution-annealing heat treatment. Developed for elevated-temperature applications, alloy 740H is typically used in the aged, precipitation-hardened

* Corresponding author at: Center for Electron Microscopy and Analysis, The Ohio State University, Columbus, OH 43212, USA.
E-mail address: mills.108@osu.edu (M.J. Mills).

https://doi.org/10.1016/j.scriptamat.2018.06.033
1359-6462/

condition [21]. In this work, it was cold-rolled in the solutionized (precipitate-free) state and subsequently heat treated, which achieved dual purposes of annealing the highly deformed microstructure to restore ductility and inducing precipitation to enhance the yield strength. This combination of chemistry and processing produced an alloy with ultra-high yield strength and large ductility.

Commercial alloy Inconel 740H was supplied by Special Metals Corporation in the solutionized condition, which consisted of a precipitate-free face-centered cubic (FCC) matrix and a low volume fraction of MC-type carbides containing primarily Nb or Ti. The material was rolled to a 65% reduction in thickness and annealed for 1 or 2 h at temperatures ranging from 600 °C–900 °C. To compare the strengthening increment from precipitation alone, material was also aged for the same times and temperatures without the intermediate rolling step. Following thermomechanical processing, tensile specimens were cut via electrical discharge machining (EDM) and tested in uniaxial tension on an Instron Electro-Thermal Mechanical Tester (ETMT) with engineering strain rates of 10^{-3} s^{-1}. Strain measurements were made using digital image correlation (DIC) with paint patterns applied to the surface of the specimens. Full-field strain maps were produced with Correlated Solutions VIC2D software using subset and step sizes of approximately 0.65 mm and 0.01 mm, respectively. Engineering strain was determined through conversion of the average Lagrangian strain in the gauge section as calculated by VIC2D.

Pre- and post-deformation specimens were characterized using an FEI Apreo scanning electron microscope (SEM) and an FEI TF-20 Tecnai 200 kV transmission electron microscope (TEM). Electron backscatter diffraction (EBSD) was performed on the SEM using an EDAX Hikari Super EBSD camera in conjunction with acquisition software EDAX TSL DC7 and analysis software EDAX TSL OIM 8. Scans were acquired using an accelerating voltage of 20 kV and a beam current of 6.4 nA at a working distance of 20 mm. The deformation structures were studied in the TEM using foils prepared via focused ion-beam (FIB) milling.

The mechanical responses produced by several selected processing conditions are shown in Fig. 1. The as-received solution-annealed specimen, which was fully recrystallized and had a large grain size of approximately 90 μm, had the lowest strength and largest ductility of any tested specimens. Note that the material was free of prior deformation and precipitates in this state. Aging the solutionized material at 900 °C for 2 h induced precipitation of the γ′ phase. Due to the modest quantities of γ′-forming elements Al and Ti, the volume fraction remained low at ~6.5% with average particle diameter 31 nm. These precipitates increased the yield strength from 300 MPa in the solutionized specimens to approximately 550 MPa. The ductility decreased but still

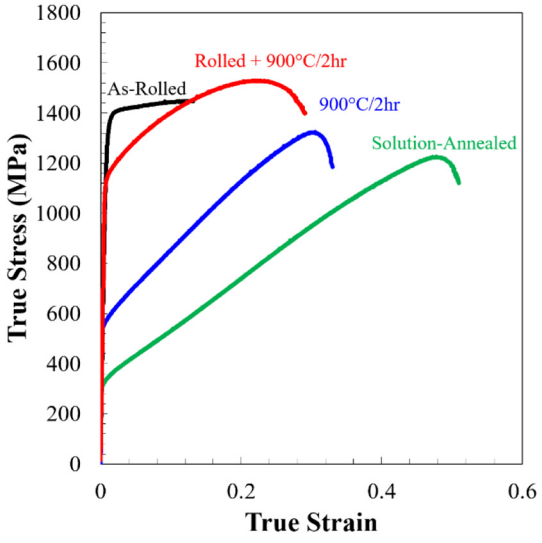

Fig. 1. Tensile true stress-strain curves for IN740H with different processing steps.

achieved a uniform elongation of about 29% (true strain) and elongation to failure of 39% (engineering strain).

The most outstanding properties were achieved for specimens that were cold-rolled and annealed at 900 °C for 1 and 2 h. All rolled samples that were annealed at temperatures below 900 °C retained properties similar to the as-rolled condition, which had very high strength but negligible uniform elongation. In contrast, rolled specimens processed at 900 °C for 2 h had an average yield strength of 1099 MPa with 15% uniform elongation and 30% elongation to failure. Note that for non-rolled and rolled specimens given the same 900 °C/2 h heat treatment, the addition of the intermediate rolling step increased the yield strength by 550 MPa (doubling the value in the non-rolled material) with only a modest change to the total elongation, from 39% to 30%.

Fig. 2 shows the microstructural evolution for specimens aged at 900 °C for 2 h with and without prior rolling. The inset inverse pole figure (IPF) triangles for each figure give the crystal orientation parallel to the specimen tensile axis, which has previously been associated with strong texture development in CrCoNi and other FCC alloys. Prior to deformation, the non-rolled specimen had large equiaxed grains with a substantial area fraction of annealing twins and no substantial texture (Fig. 2a). Deformation in uniaxial tension produced a strong double-fiber texture with ⟨111⟩ and ⟨100⟩ components parallel to the tensile axis (Fig. 2b).

In contrast, the rolled and aged specimen showed highly elongated grains with extensive intragranular rotation and deformation even after annealing (Fig. 2c). Many regions also recrystallized to form fine grains free of orientation gradients, which are marked with arrows on the inset in Fig. 2c. Although there was some evidence for residual texture with preferred orientations near ⟨111⟩, the overall texture was relatively weak due to the large fraction of recrystallized grains. After tensile deformation (Fig. 2d), the IPF maps showed large intragranular rotations with grains even more highly elongated and partitioned than in the pre-deformed state. Separation of data from the recrystallized and non-recrystallized grains clearly showed substantial rotation of the latter during the tensile experiment. This observation is critical as it suggests that even grains with considerable prior cold work retained their capacity for plastic deformation.

The remainder of this work focuses more closely on the specimens that were rolled and aged at 900 °C for 2 h, which exhibited superior mechanical properties. Fig. 3 shows a more detailed view of the microstructure immediately prior to tensile testing. These images were acquired after rolling and aging. Fig. 3a shows a higher magnification image of a region containing recrystallized grains, most of which were several microns in diameter. These did not display any preferred orientation and were primarily observed along prior grain boundaries, although some were occasionally noted in the apparent interior of other grains. Precipitation of the ordered $Ni_3(Al,Ti)$ γ′ phase also occurred during aging. Fig. 3b shows an SEM micrograph with fine γ′ precipitates revealed by etching (dark features). In non-recrystallized regions, γ′ precipitation was relatively homogeneous; however, recrystallized grains were denuded of the precipitates in the grain interiors and formed coarsened particles along grain boundaries. While not shown here for brevity, the ordered structure and composition were confirmed via superlattice reflections using selected area diffraction in the TEM. STEM energy dispersive spectroscopy also confirmed partitioning of Al and Ti co-located with reduced Co and Cr on a size scale consistent with the precipitate structure indicated in the SEM image of Fig. 3b.

At finer length scales, the residual deformation from rolling was apparent. Fig. 3c shows a bright-field STEM diffraction contrast image ([22, 23]) from a non-recrystallized region exhibiting extremely high dislocation densities. Many of the dislocations were concentrated in high-density dislocation walls, which tended to be elongated parallel to the trace of a single set of {111} planes. Imaging of individual dislocations proved difficult; but, the inset Fig. 3d gives some indication of the very high density that exists even between the ultra-high density walls. Although very fine deformation twins were observed in the rolled and